MULTIPHYSICS MODELING VOLUME 3

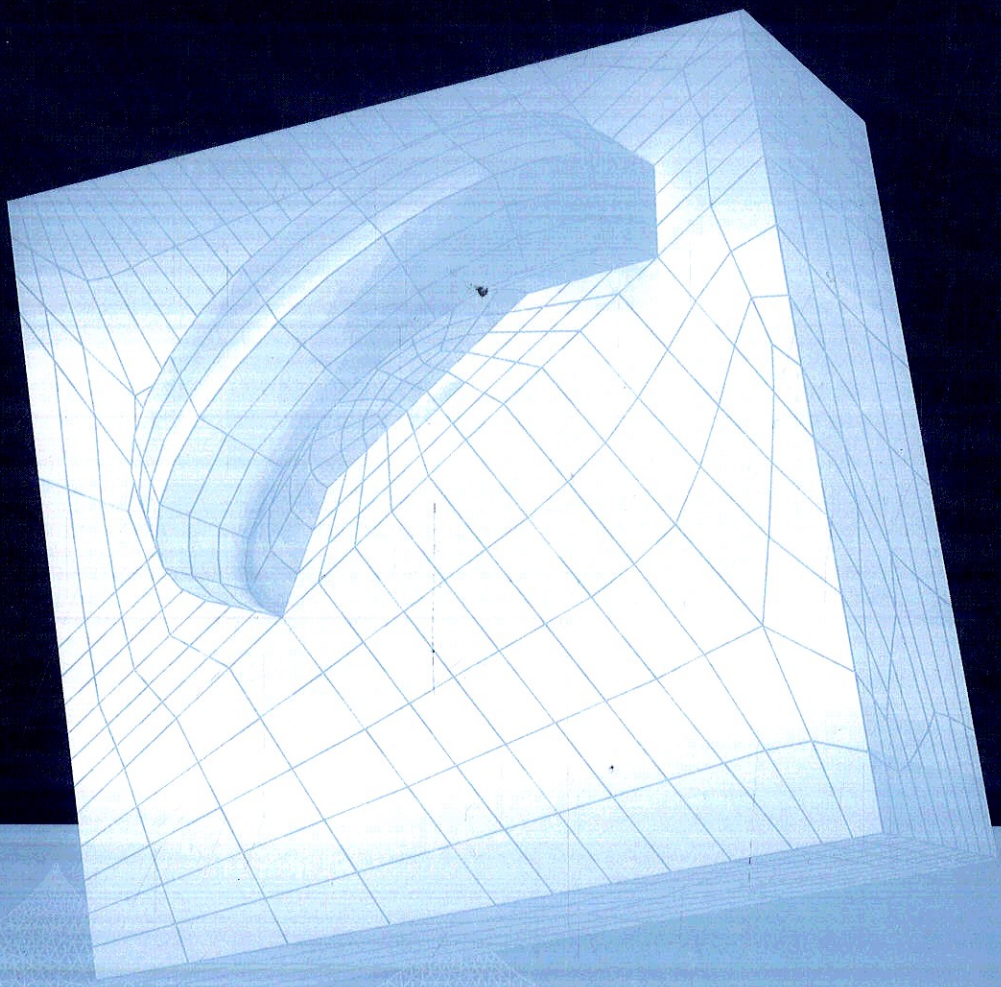

Drilling and Completion in Petroleum Engineering

Theory and Numerical Applications

Xinpu Shen, Mao Bai and William Standifird
EDITORS

CRC Press
Taylor & Francis Group
A BALKEMA BOOK

Table of contents

About the book series VII

Editorial board of the book series IX

Foreword XVII

About the editors XIX

Acknowledgements XXI

1 Mathematical modeling of thermo-hydro-mechanical behavior for reservoir formation under elevated temperature 1
1.1 Introduction 1
1.2 General conservation equations of heat and mass transfer within a deformable porous medium 2
1.2.1 Macroscopic mass conservation equations 2
1.2.2 Linear momentum conservation equations 3
1.2.3 Energy (enthalpy) conservation equations 4
1.3 Constitutive laws 5
1.3.1 Constitutive equations for mass transfer 5
1.3.1.1 Advective flow of gas 5
1.3.1.2 Advective mass flow of liquid 5
1.3.2 Constitutive equations for heat transfer 6
1.3.2.1 Conductive heat transfer within the domain Ω 6
1.3.2.2 Heat transferred in radiation at boundary $\partial\Omega$ 6
1.3.3 Constitutive equations for the mechanical response of the solid phase 6
1.4 Some empirical expressions 7
1.4.1 The expression of total porosity n 7
1.4.2 The expression of $\dot{m}_{desorp}$ 7
1.4.3 Effective thermal conductivity of the three-phase medium 8
1.5 Resultant governing equations 8
1.6 Equivalent integral of the governing differential equation and its weak form 9
1.7 Approximate solution and spatial discretization 13
1.8 Ending remarks 16

2 Damage model for rock-like materials and its application 19
2.1 Introduction 19
2.2 The Barcelona model: Scalar damage with different behaviors for tension and compression 20
2.2.1 Uniaxial behavior of the Barcelona model 20
2.2.2 Unloading behavior 21
2.2.3 Plastic flow 22
2.2.4 Yielding criterion 22
2.3 Calibration for the size of damage process zone 23
2.3.1 Experiments performed with the white-light speckle method and four-point shear beam 24

2.3.1.1 Testing device 24
2.3.1.2 Experimental results 24
2.3.2 Numerical results obtained with finite-element analysis 25
2.3.2.1 Discretization of the double-notched, four-point shear beam 27
2.3.2.2 Numerical results obtained with double notched beam 28
2.3.3 Numerical results obtained with single-notched beam 34
2.3.4 Comparisons of the experimental results with the numerical results 38
2.3.5 Remarks 38

3 Trajectory optimization for offshore wells and numerical prediction of casing failure due to production-induced compaction 41
3.1 Introduction 41
3.2 Geotechnical casing design and optimal trajectories 41
3.3 The work procedure 43
3.4 The model 44
3.4.1 Model geometry 44
3.4.2 Material models 45
3.4.3 Loads and boundary conditions of the global model 47
3.5 Numerical results of the global model 48
3.6 General principle of submodeling techniques 50
3.7 First submodel 51
3.7.1 Local model results 53
3.8 Secondary submodel and casing integrity estimate 53
3.9 Conclusions 54

4 Numerical scheme for calculation of shear failure gradient of wellbore and its applications 57
4.1 Introduction 57
4.2 Scheme for calculation of SFG with 3D FEM 58
4.3 Numerical solution of SFG and its comparison with results obtained by Drillworks 59
4.3.1 The model geometry of the benchmark and its FEM mesh 59
4.3.2 Loads and parameters of material properties 62
4.3.3 Abaqus submodel calculation and results with Mohr-Coulomb model 62
4.3.4 Results comparison with Drucker-Prager criterion between Abaqus and Drillworks 65
4.3.5 Remarks 67
4.4 Comparison of accuracy of stress solution of a cylinder obtained by Abaqus and its analytical solution 67
4.5 Application 68
4.5.1 Pore pressure analysis with Drillworks 69
4.5.2 The 3D computational model 70
4.5.2.1 Global model: Geometry, boundary condition, and loads 70
4.5.2.2 Numerical results of the global model 73
4.5.2.3 Vector-distribution of principal stresses 74
4.5.2.4 Submodel: Geometry, boundary condition, and loads 74
4.5.2.5 Numerical results of the submodel 75
4.6 Remarks 78

5 Mud weight design for horizontal wells in shallow loose sand reservoir with the finite element method 81
5.1 Introduction 81
5.2 Geological setting and geological factors affecting geomechanics 82

5.3 Pore pressure and initial geostress field: Prediction made with logging data and one-dimensional software 83
5.3.1 Pore pressure 83
5.3.2 Stress field orientation 83
5.3.3 Overburden gradient (vertical in-situ stress) 84
5.3.4 Minimum in-situ stress 84
5.3.5 Maximum in-situ horizontal stress 84
5.4 Formation strength and geomechanical properties 84
5.5 Finite element model 87
5.6 Numerical results with finite element modeling 88
5.7 Conclusions 92

6 A case study of mud weight design with finite element method for subsalt wells 95
6.1 Introduction 95
6.2 Brief review of concepts of MWW and numerical procedure for its 3D solution 97
6.2.1 Brief review of mud weight window concepts 97
6.2.2 Numerical procedure for calculating MWW with 3D FEM 99
6.3 Global model description and numerical results 99
6.3.1 Model description 99
6.3.2 Numerical results of the global model 106
6.4 Submodel description and numerical results 107
6.4.1 Model description 107
6.4.2 Numerical results of SFG and FG obtained with the secondary submodel 109
6.5 Stress pattern analysis for saltbase formation 109
6.6 Alternative validation on stress pattern within saltbase formation 115
6.7 A solution with 1D tool Drillworks and its comparison with 3D solution 115
6.8 Conclusions 117

7 Numerical calculation of stress rotation caused by salt creep and pore pressure depletion 119
7.1 Introduction 119
7.2 Stress analysis for a subsalt well 121
7.2.1 Computational model 121
7.2.2 Numerical results 122
7.3 Variation of stress orientation caused by injection and production 125
7.3.1 The model used in the computation 125
7.3.2 Numerical results 125
7.3.2.1 Numerical results of stress rotation with isotropic permeability and injection 125
7.3.2.2 Numerical results on stress rotation with isotropic permeability and production 125
7.3.2.3 Numerical results on stress rotation with orthotropic permeability and injection 127
7.3.2.4 Numerical results on stress rotation with orthotropic permeability and production 129
7.3.3 Remarks 130
7.4 Variation of stress orientation caused by pore pressure depletion: Case study in Ekofisk field 130
7.4.1 The numerical model 130
7.4.2 Numerical results 132
7.5 Conclusions 136

8 Numerical analysis of casing failure under non-uniform loading in subsalt wells 139
8.1 Introduction 139
8.2 Finite element model and analysis of casing integrity 141
8.2.1 Numerical analysis of global model at field scale 142
8.2.1.1 Model geometry 142
8.2.1.2 Material models 142
8.2.1.3 Loads and boundary conditions of the global model 144
8.2.1.4 Numerical results of global model 144
8.2.2 Submodel and casing integrity estimate 144
8.2.2.1 Model geometry 144
8.2.2.2 Material models 145
8.2.2.3 Loads specific to the submodel 146
8.2.2.4 Numerical results of the submodel: Stress distribution around the borehole before cementing 146
8.2.2.5 Numerical results of submodel: Stress distribution within the concrete ring and casing 147
8.3 Numerical results of enhancement measure 149
8.4 Conclusions 151

9 Numerical predictions on critical pressure drawdown and sand production for wells in weak formations 155
9.1 Introduction 155
9.2 Model description and numerical calculation 156
9.2.1 Numerical calculation with global model 156
9.2.1.1 Values of material parameters 157
9.2.1.2 Loads and boundary conditions of the global model 157
9.2.1.3 Stress pattern 158
9.2.1.4 Numerical results of global model 159
9.3 Case 1: Prediction of CVPDD for a well with openhole completion 159
9.3.1 Submodel 1: Geometry of the submodel 159
9.3.2 Submodel 1: Boundary condition and loads 159
9.3.3 Numerical scheme of the calculation 159
9.3.4 Numerical results 160
9.4 Case 2: Numerical prediction of CVPDD for well with casing completion 163
9.4.1 Modeling casing 164
9.4.2 Case 2A: Casing with perforation of 8 shots per 0.3048 m 165
9.4.2.1 Description of the model: Case 2A 165
9.4.2.2 Numerical results of Case 2A 166
9.4.3 Case 2B: Casing with perforation of 4 shots per 0.348 m (per ft) 166
9.4.3.1 Geometry of the model: Case 2B 166
9.4.3.2 Numerical results of Case 2B 167
9.4.4 Remarks 168
9.5 Numerical prediction of sanding production 168
9.5.1 Model description and simplifications 168
9.5.2 Numerical procedure for prediction of sand production 169
9.5.3 An example of prediction of sand production 170
9.6 Conclusions 172

10 Cohesive crack for quasi-brittle fracture and numerical simulation of hydraulic fracture 175
10.1 Introduction 175
10.2 Cohesive crack for quasi-brittle materials 175
10.2.1 Concepts of cohesive crack 175
10.2.2 Influence of hydraulic pressure on yielding conditions 176

10.2.3 Cohesive models for mixed-mode fracture 177
10.2.4 Cohesive model of effective opening for mixed-mode crack 177
10.2.5 Cohesive law formulated in standard dissipative system 179
10.2.5.1 Elastoplastic damage interface model 180
10.2.5.2 Viscoplastic interface crack model 181
10.3 Cohesive element coupled with pore pressure for simulation of hydraulic fracture of rock 181
10.3.1 Nodal sequence and stress components of cohesive element 181
10.3.2 Fluid flow model of the cohesive element 182
10.3.2.1 Defining pore fluid flow properties 182
10.3.2.2 Tangential flow 182
10.3.2.3 Newtonian fluid 183
10.3.2.4 Power law fluid 183
10.3.2.5 Normal flow across gap surfaces 183
10.4 Numerical simulation of hydraulic fracturing with 3-dimensional finite element method 184
10.4.1 Numerical procedure for the numerical simulation of hydraulic fracturing 184
10.4.2 Finite element model 184
10.4.2.1 Geometry and mesh 184
10.4.2.2 Initial conditions 184
10.4.2.3 Boundary condition 185
10.4.2.4 Loads 185
10.4.2.5 Values of material parameter 185
10.4.3 Numerical results 187
10.5 Conclusions 189

11 Special applications in formation stimulation and injection modeling 193
11.1 Introduction 193
11.2 Normal applications 194
11.3 Special applications 196
11.4 Unconventional shale gas reservoirs 196
11.4.1 Theoretical basis in simulation 196
11.4.2 An equivalent shale gas hydraulic fracturing model 197
11.4.3 Leakoff effect for a contained fracture 199
11.4.4 Concluding remarks 199
11.5 Cuttings re-injection 200
11.5.1 Theoretical basis in simulation 200
11.5.2 An equivalent cuttings re-injection model 200
11.5.3 Key input parameters for cuttings re-injection modeling 201
11.5.4 Multiple fracture modeling 202
11.5.5 Net pressure responses in cyclic injection 204
11.5.6 Concluding remarks 206
11.6 Fracture packing in unconsolidated formation 206
11.6.1 Theoretical basis in simulation 206
11.6.2 An equivalent frac-pack model 206
11.6.3 Key input parameters for frac-pack modeling 208
11.6.4 Fracture re-growth during the frac-pack process 208
11.6.5 Concluding remarks 211
11.7 Produced water re-injection 212
11.7.1 Theoretical basis in simulation 212
11.7.2 An equivalent produced water re-injection model 212
11.7.3 Numerical modeling of cross flow in produced water transport 213

11.7.4 Analytical modeling of cross flow and its effect on produced water transport 218
11.7.5 Concluding remarks 219

Subject index 221

Book series page 233